ECS Journal of Solid State
Science and Technology

Broadened Bandwidth Amplified Spontaneous Emission from Blue GaN-Based Short-Cavity Superluminescent Light-Emitting Diodes

ECS Journal of Solid State Science and Technology, 2020 **9** 015019

Broadened Bandwidth Amplified Spontaneous Emission from Blue GaN-Based Short-Cavity Superluminescent Light-Emitting Diodes

Hezhi Zhang, Ching-Wen Shih, Denis Martin, Alexander Caut, Jean-François Carlin, Raphaël Butté, and Nicolas Grandjean [z]

Institute of Physics, École Polytechnique Fédérale de Lausanne (EPFL), CH-1015 Lausanne, Switzerland

We report broad bandwidth blue superluminescent light-emitting diodes (SLEDs) based on a short-cavity active region. The dependencies of amplified spontaneous emission (ASE) output power and gain bandwidth on cavity length were investigated in devices whose gain medium consists of a ridge waveguide with embedded InGaN/GaN quantum wells sandwiched between one etched facet coated with a high reflectivity distributed Bragg mirror and one cleaved facet with an anti-reflection coating. 250 μm-long blue SLEDs exhibit a spectral bandwidth up to 7.5 nm at 1.72 mW output power at a wavelength of 427 nm. As cavity length decreases, the bandwidth gradually broadens up to 15 nm for the shortest, 40 μm-long, SLED devices. ASE is confirmed by current-dependent electroluminescence spectra and polarization-dependent emission intensity measurements. The optical features of those short-cavity devices could be helpful for designing broad bandwidth SLEDs aiming for various applications such as optical coherence tomography, next generation displays, on-chip biosensing and imaging.

 [DOI: 10.1149/2.0432001JSS]

Manuscript submitted October 17, 2019; revised manuscript received November 18, 2019. Published December 16, 2019. *This paper is part of the JSS Focus Issue on Recent Advances in Wide Bandgap III-Nitride Devices and Solid State Lighting: A Tribute to Isamu Akasaki.*

Since the first demonstration of high-brightness GaN-based blue light-emitting diodes (LEDs),[1] blue LEDs and laser diodes (LDs) have been massively commercialized and play nowadays an important role in the markets of illumination, data storage, etc. Despite the rapid advancement made with blue LEDs and blue LDs, it was not until 2009 that the first III-nitride (III-N) blue superluminescent light-emitting diodes (SLEDs) were reported.[2] SLEDs typically inherit their index-guided ridge waveguide (WG) geometry from LDs, while introducing an anti-reflection (AR) coating,[3] a passive absorber[4] or an oblique facet on one end of the WG to suppress lasing action.[5,6] The temporal incoherence conjugated with spatial coherence guarantee SLEDs to emit highly directional beams characterized with a broad bandwidth, thereby enabling speckle-free images, which is suitable for pico-projection, fiber optic gyroscope (FOG), or optical coherence tomography (OCT) applications. Previously, many efforts have been devoted to the increase of the output power of SLEDs for pico-projection and FOGs; applications for which a modest spectral bandwidth is required. As a consequence, the cavity length is designed to be longer than 500 μm to promote amplified spontaneous emission (ASE), leaving the full width at half maximum (FWHM) to less than 5 nm in InGaN-based SLEDs.[6,7] However, the situation is different for OCT applications. Indeed, SLEDs emitting at short wavelengths with a broad spectral bandwidth could be more favorable for OCT over high power ones, as the lateral resolution is proportional to $\lambda^2/\Delta\lambda$, where λ is the central wavelength and $\Delta\lambda$ is the FWHM of the ASE spectrum.[8,9] Furthermore, developing broad bandwidth ultrashort cavity devices working at high current density could generate superradiance emission, hence leading to ultrashort light pulses with duration down to the picosecond.[10]

In this work, we develop broad bandwidth InGaN-SLEDs based on short-cavity devices. The device design is guided by a trade-off between optical power and ASE bandwidth:[11,12] the longer the cavity length, the higher the output power at a fixed current density, and the narrower the ASE bandwidth.

Growth and Processing Details

SLED epilayers were grown on 2-inch freestanding *c*-plane GaN substrate (dislocation density $\sim 10^6$ cm^{-2}) by metal organic chemical vapor deposition in an Aixtron 3 × 2 in. CCS system. The epitaxial structure consists of an *n*-type doped GaN buffer, a 910 nm thick Si-doped *n*-type $Al_{0.06}Ga_{0.94}N$ cladding layer, and a 3-period $In_{0.12}Ga_{0.88}N$(4.7 nm)/GaN(12 nm) quantum well (QW) embedded within a GaN WG aiming for an emission at 425 nm. The *p*-type doped layers consist of a 20 nm thick $Al_{0.2}Ga_{0.8}N$ electron blocking layer, a 460 nm thick Mg-doped $Al_{0.06}Ga_{0.94}N$ cladding (N_A-N_D $\sim 1 \times 10^{19}$ cm^{-3}), and an 80 nm thick highly Mg-doped (N_A-N_D $\sim 2 \times 10^{19}$ cm^{-3}) GaN contact layer.

After *p*-type GaN activation and 10-minute deoxidization in HCl solution at 80°C (Fig. 1a), the epiwafers were processed into short-cavity SLED devices. First, the epiwafers are metallized (Fig. 1b) and 1.5 μm deep etching is performed by chlorine-based inductively coupled plasma (ICP) (Fig. 1c). Afterwards, etched-sidewalls are treated in a potassium hydroxide (KOH) based solution to obtain smooth facets. The next steps deal with the ICP etching of 3 μm wide ridges (Fig. 1d), the deposition of a silicon dioxide (SiO_2) isolation layer (Fig. 1e), *p*-contact ridge opening (Fig. 1f), and *n*-contact deposition (Fig. 1g). Then, a high-reflection coating consisting of an eight-pair SiO_2 (72 nm) /ZrO_2 (50 nm) distributed Bragg reflector (DBR) is deposited on the facets (Fig. 1h). The whole processing is terminated by the cleavage of the epiwafers along deep trenches, which are introduced in order to form cavities whose length varies from 250 μm down to 40 μm (Fig. 1i). More details about the processing can be found in our previous work.[13]

Experimental Results and Discussion

After processing, the electrical and the optical properties of a 250-μm long reference LD device were first characterized. From the typical continuous wave (cw) light output (*L-I*) characteristics shown in Fig. 2a, a lasing threshold current of 88 mA followed by a steep power increase up to 55 mW at 165 mA is measured, hence leading to a slope efficiency (η_s) of 0.71 W/A. The lasing spectrum is centered at 427 nm for a current of 100 mA.

To avoid any lasing action, another part of the same epilayer was processed into SLEDs by depositing an AR coating having a reflectivity (*R*) below 1% on the cleaved facet. The *R* value was estimated by depositing the same AR coating on a reference planar GaN wafer, measuring *R* with a Cary 500 spectrophotometer and comparing the measured spectra to transfer matrix simulations. The total output power (Fig. 3a) of 250-μm long short-cavity SLEDs exhibits a superlinear increase reaching up to 3.2 mW at 220 mA under cw injection condition. To extract the contribution of ASE to the total output power, we recorded the electroluminescence (EL) spectra with an optical fiber from both the front output facet (Fig. 3b) and the top of the ridge (Fig. 3c). Indeed, the light that propagates along the ridge WG is mostly

[z]E-mail: nicolas.grandjean@epfl.ch

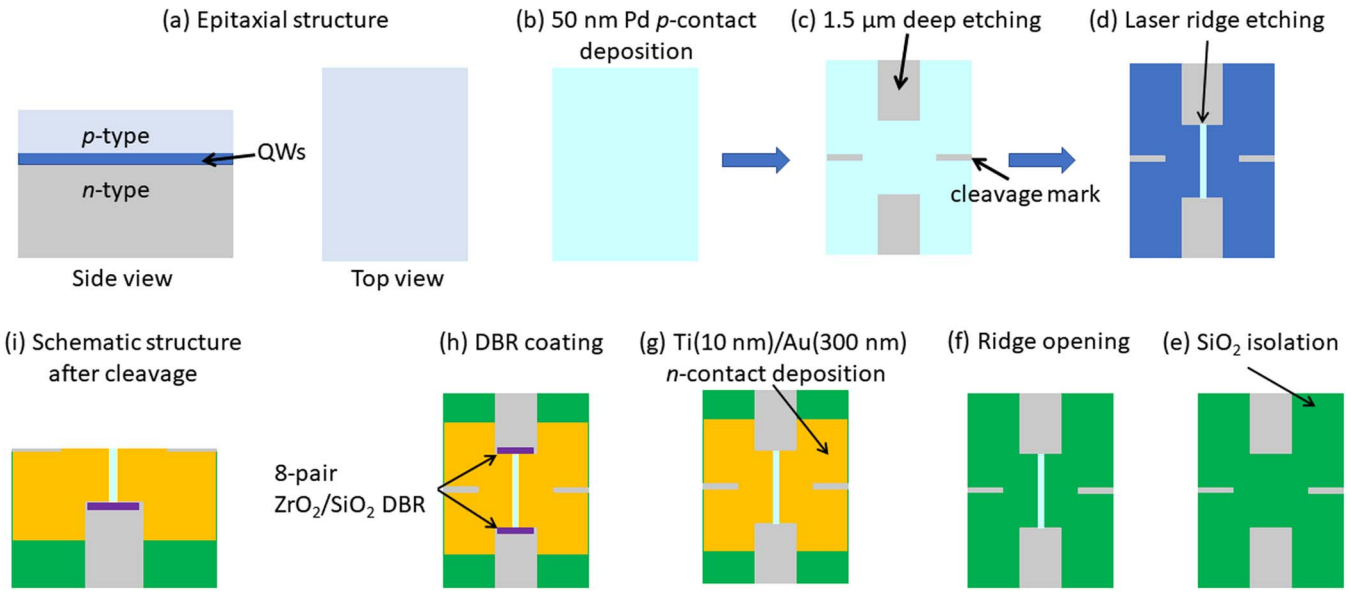

Figure 1. Schematics of the process flow used for the fabrication of short-cavity SLED devices.

proportional to the ASE rate whereas the top emission is dominated by the spontaneous emission (SE) rate. It originates from the fact that the latter is marginally coupled to the WG mode in such ridge WG geometry, a well-known feature of SLEDs.[2,14] The SE and ASE power in the *L-I* characteristics can be properly scaled so that the summation shown as the red solid dots in Fig. 3a can uniquely fit the measured power shown as the blue curve over the whole injection current range. As deduced from the fitting results, for driving currents below 37.5 mA, the output power is dominated by SE. As injection increases, the ASE output power grows exponentially and finally exceeds the SE power at a current of 190 mA, reaching 1.72 mW at 220 mA. Typical ASE characteristics of SLEDs such as spectral narrowing from ~25 nm at 10 mA to 7.5 nm at 215 mA, due to the transition from the spontaneous emission regime to the optical gain one (Fig. 3d),[14] and peak emission wavelength blueshift from 435 nm to 427 nm are observed. This emission blueshift with increasing driving current, which is also visible in SE EL spectra, is the usual manifestation of the progressive screening of the built-in electric field, i.e., the quenching of the quantum confined Stark effect, inherent to polar III-N quantum heterostructures with increasing carrier density.[15] From a driving current exceeding ~90 mA (12 kA/cm^2) the reported redshift in the SE and ASE EL spectra is likely due to self-heating issues. However, quantifying the physical origin of the different rates in the shifts at high current is beyond the scope of the present work. It could potentially involve complex many body phenomena that affect the shape of the gain band.

To determine the role of the cavity length on the optical properties of blue SLEDs, their edge-emitted EL spectra were recorded under cw injection condition for cavity lengths varying between 250 μm and 40 μm (Fig. 4a). For the sake of consistency, the corresponding FWHM are compared at the same current density of 30 kA/cm^2. We observe a larger ASE linewidth with decreasing cavity length, a spectral feature also reported for near-infrared SLEDs.[12] The latter can essentially be understood by the fact that, in a Fabry-Perot (FP) device such as the present SLEDs, the gain bandwidth scales as the inverse of cavity length, as shown in the case of semiconductor optical

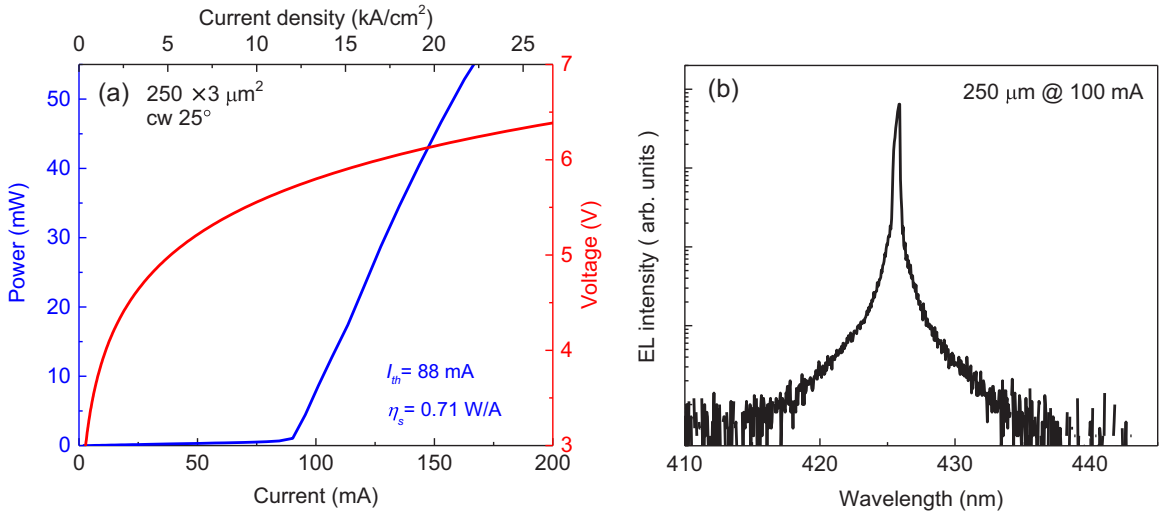

Figure 2. (a) Current-voltage (*I-V*) and *L-I* curves measured on a reference 250-μm long LD under cw injection exhibiting a threshold current at 88 mA and η_s of 0.71 W/A. (b) Corresponding cw EL spectrum recorded at 100 mA.

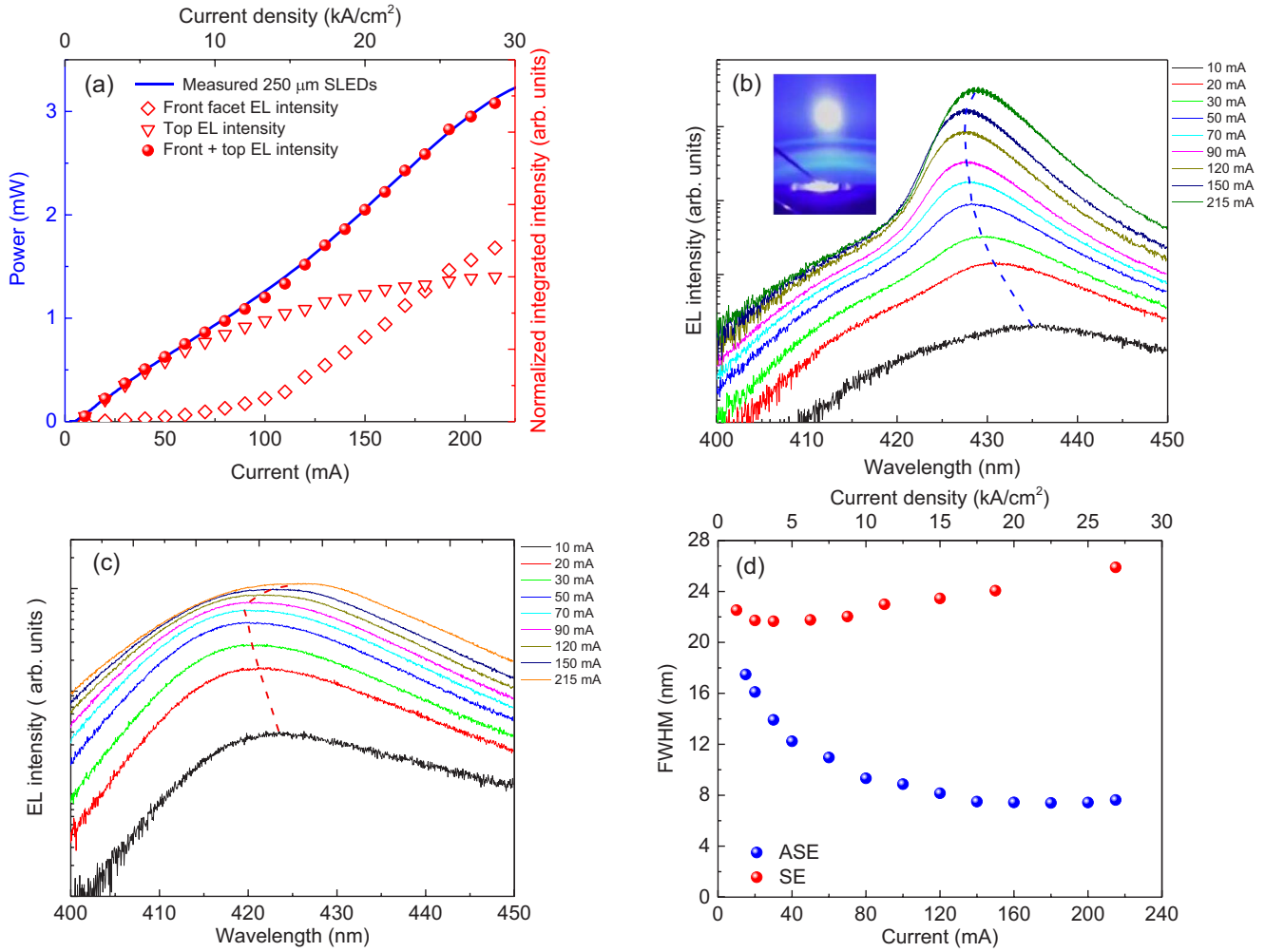

Figure 3. (a) *L-I* curve (red dots) of a 250-μm long SLED recorded under cw injection exhibiting a superlinear increase. The fraction of ASE and SE is indicated by open diamonds and open triangles, respectively. (b) Current-dependent EL spectra emitted through the AR-coated front facet. The blue dashed line shows the evolution of the peak emission wavelength with increasing driving current. The inset of (b) indicates the typical far-field emission pattern of 250-μm long SLEDs. (c) Current-dependent top emitted EL spectra and evolution of the corresponding peak emission wavelength with increasing driving current (red dashed line). (d) FWHM of ASE (blue dots) and SE (red dots) spectra as a function of driving current for a 250-μm long SLED showing ASE narrowing down to 7.5 nm.

amplifiers,[16] due to the decrease in the quality factor of the FP cavity. The ASE linewidth eventually reaches a value of 15 nm for the shortest investigated devices, which are 40-μm long. The corresponding EL spectrum and the associated far-field emission pattern indicating a speckle-free directional beam are shown in the inset of Fig. 4a and in Fig. 4b, respectively.

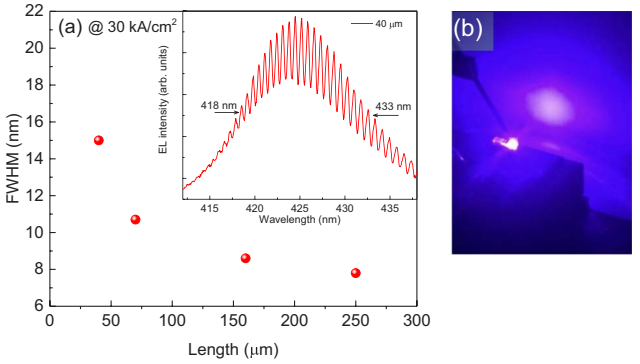

Figure 4. (a) ASE FWHM as a function of cavity length showing a broadened bandwidth to 15 nm for a 40-μm long SLED device. Inset: Edge-emitted EL spectrum of a 40-μm long SLED device recorded at 30 kA/cm² showing FP resonances typical of ASE. (b) Far-field emission pattern of a 40-μm long SLED device.

To examine whether the 15 nm FWHM emission can be exclusively attributed to ASE instead of SE, we characterized the electrical and optical properties of a representative 40-μm long device. From the *I-V* behavior (Fig. 5a, red curve), this device exhibits a stable and efficient electrical injection up to 35 kA/cm² in cw mode. Nevertheless, the *L-I* characteristics (Fig. 5a, blue curve) does not show a typical superlinear increase in output power. To get additional insights, we monitored the evolution of current density dependent EL spectra recorded from the output facet (Fig. 5b) together with the linear degree of polarization (DOP) (Fig. 5c). The front facet EL spectra of the 40-μm long device display a behavior quite similar to that of standard 250-μm long devices, i.e., a narrowing of the ASE FWHM from 25 nm to 15 nm when the driving current increases from 1 to 42 mA, and a simultaneous peak emission wavelength blueshift from 435 to 425 nm due to the progressive screening of the built-in electric field. Such a signature is typical of ASE, which is further confirmed by the DOP measurements. At a current of 30 mA, the DOP exhibits an enhanced transverse electric (TE) polarization with a polarization mode intensity ratio (TE-TM)/(TE+TM), with TM the transverse magnetic mode intensity, as high as 0.97, which is in agreement with similar studies indicating that TE mode emission dominates over the TM one in InGaN-based LDs, LEDs and SLEDs.[17–19] TE- and TM-polarized EL spectra

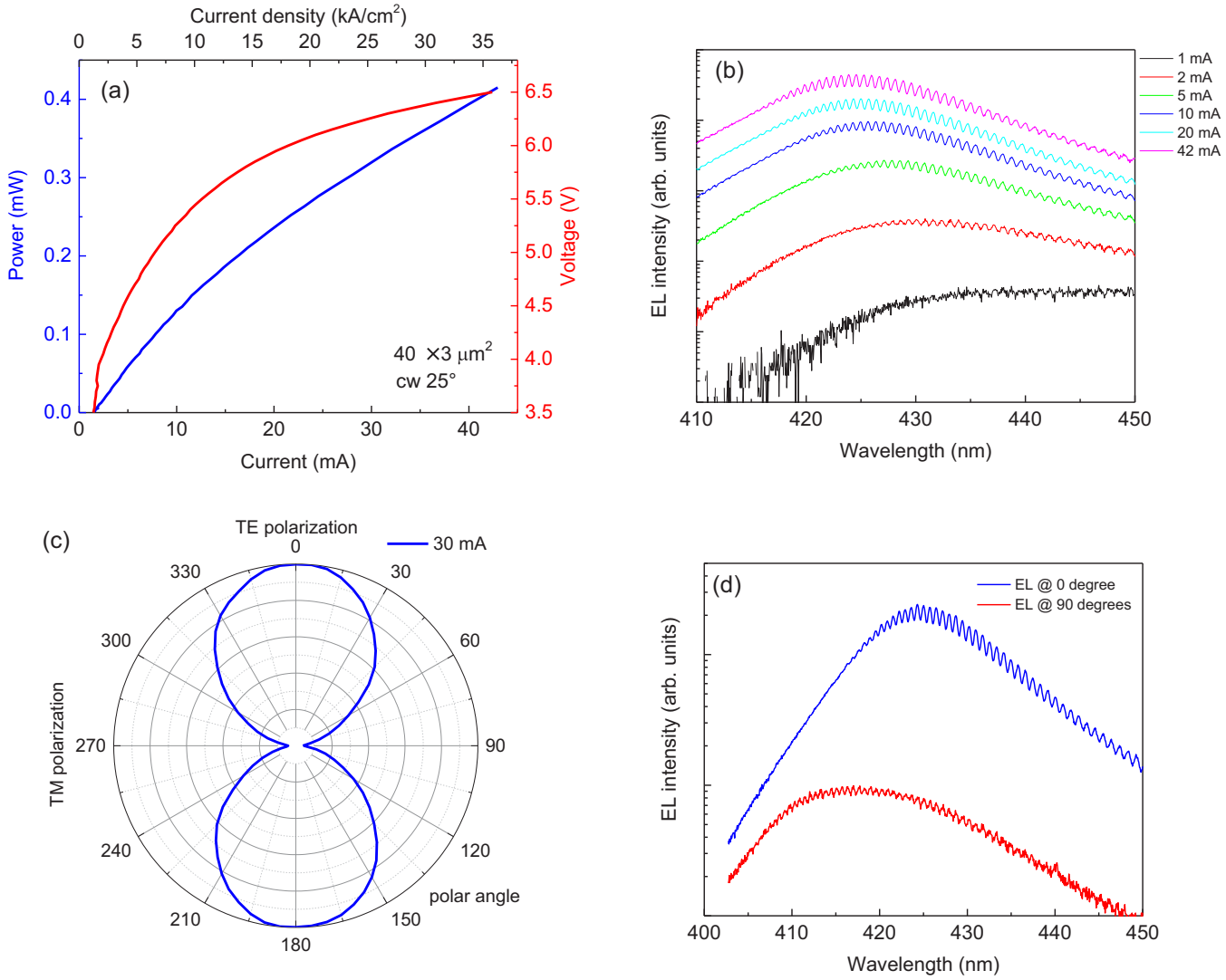

Figure 5. (a) *I-V* and *L-I* curves of a 40-μm long SLED device measured under cw injection. (b) Current dependent EL spectra recorded at the output of the AR coated facet. (c) DOP measurement at a driving current of 30 mA showing the TE-dominated polarization of the emitted light. (d) TE- and TM-polarized EL spectra.

corresponding to polarization angles of 0 and 90 degrees, respectively, are displayed in Fig. 5d. Let us note that the present optical polarization signature is most likely originating from the compressive strain experienced by the *c*-plane grown InGaN/GaN QW gain medium that favors optical transitions involving the A and B valence subband states, which are preferentially coupled to TE modes for the ridge WG emission.[18] On the contrary, TM modes are mostly related to optical transitions involving the C valence subband, which obviously emits at higher energy, hence explaining the blueshift of TM polarized light versus TE one.[18] The observed sublinear shape of the *L-I* curve is attributed to the low fraction of ASE contribution into the total output power.

Conclusions

In conclusion, we developed broad bandwidth blue emitting SLEDs based on short-cavity devices of length ranging from 250 μm down to 40 μm. The ASE output power of 250-μm long SLEDs reaches values up to 1.72 mW at a cw driving current of 220 mA together with a 7.5 nm FWHM ASE spectrum, which is a promising figure of merit for OCT applications. As the cavity length is decreased down to 40 μm, the corresponding ASE FWHM shows a significant increase up to a value of 15 nm. However, this is obtained at the expense of the output power. Improvement on both the processing and the epitaxial structure side should allow achieving short-cavity SLEDs with decent output power and linewidth in excess of 10 nm.

Acknowledgments

This work was supported by EU Horizon H2020 project SUPER-TWIN (id686731).

ORCID

Nicolas Grandjean https://orcid.org/0000-0003-3610-981X

References

1. S. Nakamura, T. Mukai, and M. Senoh, *Appl. Phys. Lett.*, **64**, 1687 (1994).
2. E. Feltin, A. Castiglia, G. Cosendey, L. Sulmoni, J.-F. Carlin, N. Grandjean, M. Rossetti, J. Dorsaz, V. Laino, M. Duelk, and C. Vélez, *Appl. Phys. Lett.*, **95**, 081107 (2009).
3. M. Rossetti, J. Dorsaz, R. Rezzonico, M. Duelk, C. Velez, E. Feltin, A. Castiglia, G. Cosendey, J.-F. Carlin, and N. Grandjean, *Appl. Phys. Express*, **3**, 061002 (2010).
4. C. Shen, T. K. Ng, J. T. Leonard, A. Pourhashemi, S. Nakamura, S. P. DenBaars, J. S. Speck, A. Y. Alyamani, M. M. El-Desouki, and B. S. Ooi, *Opt. Lett.*, **41**, 2608 (2016).
5. F. Kopp, C. Eichler, A. Lell, S. Tautz, J. Ristic, B. Stojetz, C. Hoss, T. Weig, U. T. Schwarz, and U. Strauss, *Jpn. J. Appl. Phys.*, **52**, 08JH07 (2013).

6. A. Kafar, S. Stanczyk, G. Targowski, T. Oto, I. Makarowa, P. Wisniewski, T. Suski, and P. Perlin, *Appl. Phys. Express.*, **6**, 092102 (2013).
7. A. Castiglia, M. Rossetti, N. Matuschek, R. Rezzonico, M. Duelk, C. Vélez, J.-F. Carlin, and N. Grandjean, *Proc. SPIE*, **9748**, 97481V (2016).
8. A. Kafar, S. Stańczyk, M. Sarzyński, S. Grzanka, J. Goss, G. Targowski, A. Nowakowska-Siwińska, T. Suski, and P. Perlin, *Opt. Express*, **24**, 9673 (2016).
9. Y. Deng and D. Chu, *Sci. Rep.*, **7**, 5893 (2017).
10. G. Timothy Noe II, J.-H. Kim, J. Lee, Y. R. Wang, A. K. Wojcik, S. A. McGill, D. H. Reitze, A. A. Belyanin, and J. Kono, *Nat. Phys.*, **8**, 219 (2012).
11. M. Rossetti, J. Napierala, N. Matuschek, U. Achatz, M. Duelk, C. Vélez, A. Castiglia, N. Grandjean, J. Dorsaz, and E. Feltin, *Proc. SPIE*, **8252**, 825208 (2012).
12. N. Matuschek and M. Duelk, *IEEE J. Sel. Top. Quantum Electron.*, **19**, 7800307 (2013).
13. H. Zhang, C.-W. Shih, D. Martin, A. Caut, J.-F. Carlin, R. Butté, and N. Grandjean, *Semicond. Sci. Technol.*, **34**, 085005 (2019).
14. T.-P. Lee, C. A. Burrus, and B. I. Miller, *IEEE J. Quantum Electron.*, **9**, 820 (1973).
15. V. Fiorentini, F. Bernardini, F. Della Sala, A. Di Carlo, and P. Lugli, *Phys. Rev. B*, **60**, 8849 (1999).
16. T. Mukai and Y. Yamamoto, *IEEE J. Quantum Electron.*, **17**, 1028 (1981).
17. G. Frankowsky, F. Steuber, V. Härle, F. Scholz, and A. Hangleiter, *Appl. Phys. Lett.*, **68**, 3746 (1996).
18. C. Jia, T. Yu, S. Mu, Y. Pan, Z. Yang, Z. Chen, Z. Qin, and G. Zhang, *Appl. Phys. Lett.*, **90**, 211112 (2007).
19. F. Kopp, T. Lermer, C. Eichler, and U. Strauss, *Appl. Phys. Express.*, **5**, 082105 (2012).